Content

List of Figure

List of Table

List of Acronyms

PBG   photonic band gap

PC   photonic crystal

PML   perfectly matched layer

CB   conduction band edge

VB   valence band edge

Nomenclature

$\eta(\mathbf{r})$: the square inverse of the permittivity distribution

$\hat{O}$: the eigen operator for the Wannier envelope function

$\Gamma(\mathbf{r})$: the envelope function

λ : the eigenvalue for the Wannier envelope function

$\mathbf{k}_X$: the position vector of point X in k space of the triangular lattice

f   : the filling factor

r   : the radius of the air hole s

a   : the conventional lattice constant

S_x : the stretched parameter

Sx   : the imaginary part of the stretched parameter

x_{pml} : the position of the interface of the PML

x_{well} : the position of edge of the potential well

L   : the total length of the system

$\Delta\Gamma'(\mathbf{r})$: the envelope of the effective Wannier potential distribution

$m*$: The effective mass

w_{pml} : the thickness of the PML

1.　　Introduction

1.1　　Motivation

The concept of photonic band gap (PBG) has been one of the most popular topics in recent photoelectronic development. Photonic crystal (PC) is widely utilized to enhance the optical properties of single mode light emitting diodes, add-drop filters, low loss waveguide bends, polarization selectors, planar antenna substrates and semiconductor lasers. The future of photonic crystals is unequivocally bright. We can foresee highly efficient photonic crystal lasers and extremely bright LEDs (light emitting device) entering the marketplace. Photonic crystal diodes and transistors, and even a simple logic circuit for a prototype optical computer are envisioned to be demonstrated in at most 30 years.

In addition, the slab waveguide with a 2D photonic crystal lattice structure is

one of the popular candidates to be fabricated following the standard microlithographic techniques. The triangular PC lattice with single defect is drilled on the chosen slab to form a resonant cavity. In 1999, an optically pumping laser made of an InGaAsP slab with a single defect 2D PC pattern was experimentally demonstrated [1]. Many works on simulating the aforementioned structure have been published [2].

However, due to the massive computational cost, the topic of an efficient artificial absorbing medium to simulate the unbounded system is also attractive. Under urgent requirement is an absorbing boundary condition (ABC) with reflectionless absorption of incident waves, regardless of incident angle or wavelength. To the end, the stretched perfectly matched layer (PML) introduced by Chew [3], *et al.*, is suitable for this purpose and for the case under discussion now.

In this thesis, we will employ a simple but powerful method, which is different from those introduced by others, to treat the perfectly matched layer. A wave equation, that is the envelope of the resonant optical modes of local defects within two-dimension periodic dielectric structures, coupled the attenuator parameter- stretched parameter, is derived. The states inside the cavity, including guided and bounded states, can be easily found, and have the eigenvalues increasing with a reasonable way.

1.2   Literature review

At the very beginning, the concepts of pohotonic band-gap can be traced back to 1946 when Edward Purcell [4] described the modification of the coupling of matter to the electromagnetic field by placing the system in a cavity. Almost forty years latter Kleppner [5] reinvestigated the idea of cavity modification of spontaneous emission, and latter in 1987, Yablonovitch [6] applied these concepts to the modification of the spontaneous emission in photonic band gap materials [7]. Thereafter, the blooming of research works around the world has begun. Owing to the inherent size scale, initial studies were focused on cavity structures for microwave devices [8]. With the maturation of nanometer-size photonic crystal fabrication in semiconductors [9] and other dielectrics [10], there has been intensive interest in creating optical micro-cavities for spontaneous emission control.

Many methods were used to simulate the complex distributions of the electromagnetic fields in photonic crystal structures. For reducing intensive computational cost, various absorbing boundary media have been introduced. For example, with the aim of synthesizing an absorbing boundary medium for the finite-difference time domain (FDTD) method, the perfectly matched layer was firstly introduced by Berenger and treated using the so-called split-field equation [11] in 1994. Chew and Weedon [3], and Rappapot [12]

then independently modified Berenger's split-field equation and gave a more compact and nonsplit form. This nonsplit form of PML formulations was named stretched-coordinate formulation after the attenuator parameter derived in split form. Mittra and Pekel kept the split form of Berenger's equations and converted them to the frequency domain for the application of the finite element method (FEM) in 1995 [13]. Unitil now there has been much research on the FDTD or FEM method, following their innovative works and still proceeding.

In order to illustrate the above description, we searched for the number of journal and conference articles on PML and PC for the past decade. Fig.1 shows the increase in the number of the PML- or PC-related articles with time. The data were obtained by searching in *ISI web of science*® using the key words "PML", "Perfectly matched medium", "PC", or "PBG". As can be seen from the figure, the number of papers on PC is growing exponentially. Only in 2003, the number has exceeded 500 which is the upper limit set by the ISI system.
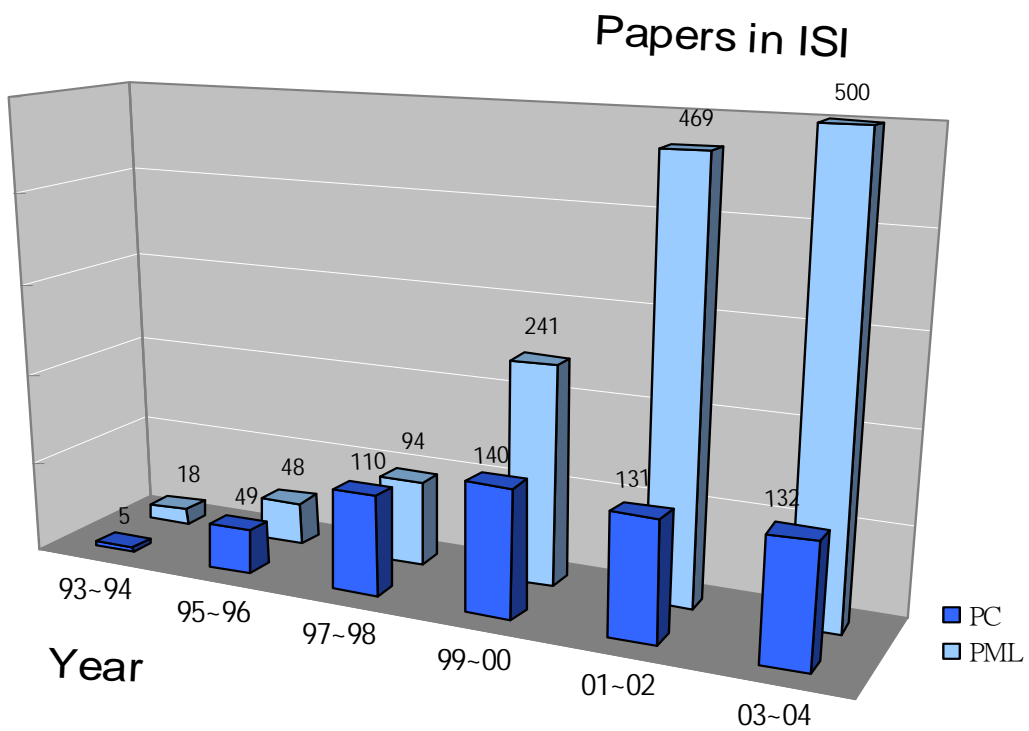
FIG 1 The papers with the topics of "PML" and "PC" in *ISI web of science*®

1.3   Organization

This thesis is divided into five sections. Section 1 introduces the background and the intuitive concepts. Section 2 resolves all the settings and formulations associated with the PC structure. Mainly, following O. Painter's work [14], a wave equation with a Wannier-like potential distribution for resonant modes of local defects in the PC medium is described. In the section 3, adopting the stretched PML concept, a novel wave equation for the envelope function of localized defect modes is proposed. The simulation results presented in section 4 will demonstrate the capability of the perfectly matched absorbing medium coupled with the Wannier-like method for simulating the defect modes of the 2D PC triangular lattice. Finally, total work is summarized and some simulation results and issues are concluded.

2.   Photonic crystal

Now, finding a Wannier—like equation [15] for the envelope of localized photon states in triangular dielectric lattices is the main topic. Of most interest are the localized resonant modes of planar 2D PCs formed in optically thin dielectric slabs. In what follows, only the TE-like modes are under focus:
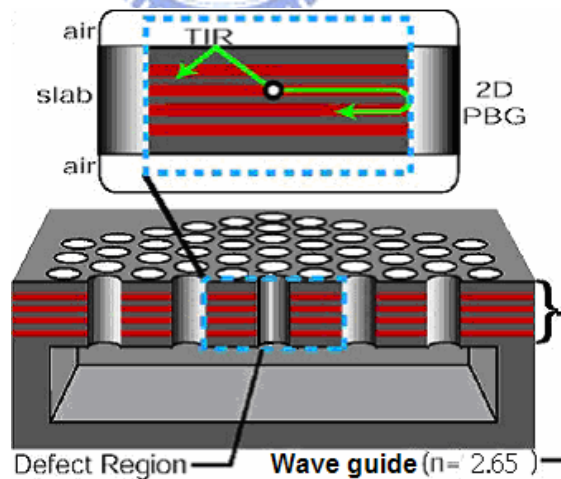
FIG 2   The structure of the PC structure. The vertical and in-plane optical confinement for the slab waveguide is shown. Besides, the effective refractive index of the slab is 2.650. (This picture is after O. Painter's paper [14].)

7

2.1   2D PC triangular lattice slab waveguide

At beginning, the Maxwell's equations in a lossless delectric medium free of currents and free charge are shown as:

$$
\begin{aligned}
\nabla \times \mathbf{E}(\mathbf{r}) &= -i\omega\mu_0\mathbf{H}(\mathbf{r}), \\
\nabla \times \mathbf{H}(\mathbf{r}) &= i\omega\varepsilon_0\varepsilon_r(\mathbf{r})\mathbf{E}(\mathbf{r}), \\
\nabla \cdot \mathbf{E} &= 0, \\
\nabla \cdot \mathbf{H} &= 0,
\end{aligned}
\tag{2.1}
$$

where electric and magnetic fields are the harmonic complex fields with time dependence $e^{i\omega t}$. Assuming that this material is non-magnetic, i.e. ,

$$
\mu(\omega,\mathbf{k},\mathbf{r}) = \mu_0
$$

and the dielectric function does not depend on spatial or temporal frequency,

$$
\begin{aligned}
\varepsilon(\omega,\mathbf{k},\mathbf{r}) &= \varepsilon_0\varepsilon_r(\mathbf{r}) \\
&= \varepsilon_0\, \mathrm{n}^2(\mathbf{r}).
\end{aligned}
\tag{2.2}
$$

From above Maxwell's equations, we find a wave equation for magnetic fields

$$\nabla \times \eta(\mathbf{r})\nabla \times \mathbf{H}(\mathbf{r}) = \frac{\omega^2}{\varepsilon_0 \mu_0}\mathbf{H}(\mathbf{r})$$

$$= \frac{\omega^2}{c^2}\mathbf{H}(\mathbf{r}) \; , \tag{2.3}$$

where the square inverse of relative dielectric function is as:

$$\eta(\mathbf{r}) \equiv \frac{1}{n^2(\mathbf{r})}, \tag{2.4}$$

and the light velocity is

$$c = 1/\sqrt{\varepsilon_0 \mu_0}.$$

Here, the 2D situation is extended to a quasi-2D system consisting of weak vertical guiding, realizing that this case is only an approximate theory which neglects polarization mixing and all out-of-plane effects.

Then, it starts at the TE modes in which the magnetic field is described by a scalar field, $\mathbf{H} = \hat{z}H$.

The Hermitian eigenvalue equation which results from Eq. (2.3) and $\nabla \cdot \mathbf{H} = 0$ is

$$\hat{O}_H^{TE}H = \lambda H, \tag{2.5}$$

with the TE eigenoperator given by

$$\hat{O}_H^{TE} = -\eta(\mathbf{r})\nabla^2 - \nabla\eta(\mathbf{r})\cdot\nabla \qquad (2.6)$$

The eigenvalue, λ, is related to the square of the frequency of the mode.

The triangular lattice specifies the periodicity of the host dielectric medium (see Fig. 3). Fig. 4 shows the fundamental TE-like guided mode band structure ($r/a=0.380, n_{eff} = n_{slab} = 2.650$), where the light line is shown as a solid yellow line.
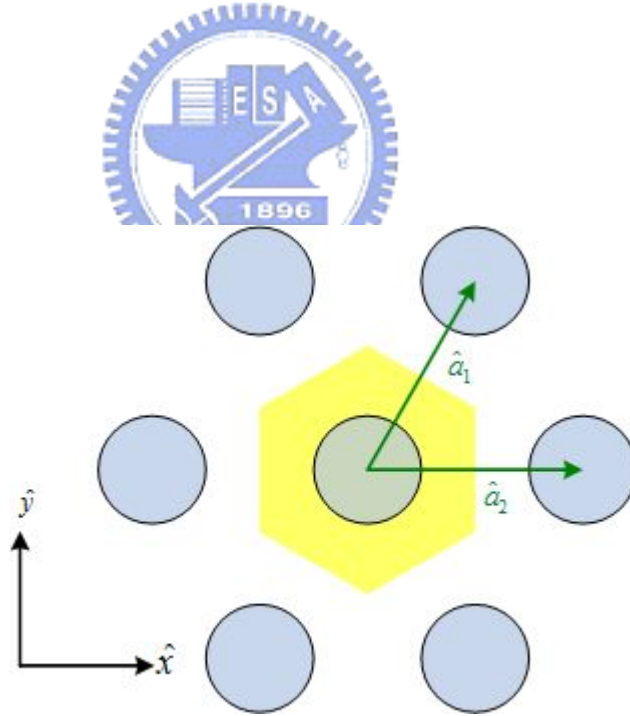
FIG 3   Illustration of the real spaces of the 2-D triangular PC ($\left|a_1\right| = \left|a_2\right| = a$)

And, what should be mentioned is that, the vertical guiding applies the effective index method [16]. So, the refractive index, n0, in the material of this kind is 2.650.
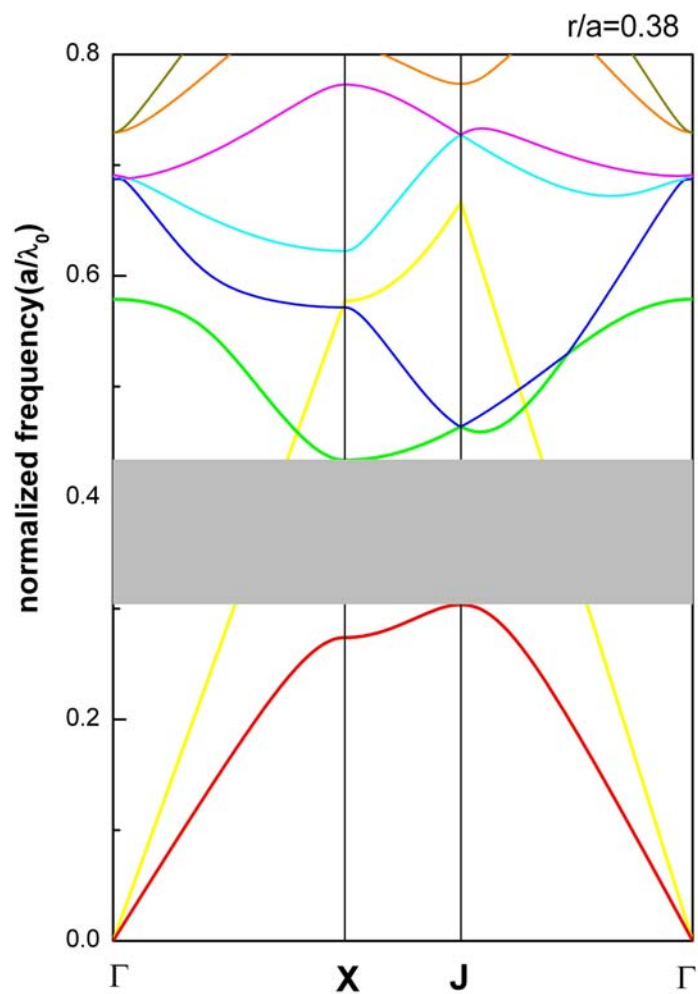
FIG 4   The fundamental TE-like guided mode band structure (r/a=0.380, $n_{eff} = n_{slab} = 2.650$)

2.2　Wannier—like equation for defect modes

An optically thin dielectric slab surrounded by the air and patterned with a 2D triangular array of holes defined the resonant cavity here (see Fig.2). The fundamental TE-like even mode with an absolute frequency band gap is considered. The development for the Wannier equations of this case will begin as a scalar field eigenvalue equation, Eq. (2.5), for the magnetic field in the quasi-2D approximation [14]. Where the eigenoperator from the Maxwell's equations is

$$\hat{O}_H^{TE} = -\nabla^2 \left[\eta_0(\mathbf{r}) + \Delta\eta(\mathbf{r})\right] - \nabla\left[\eta_0(\mathbf{r}) + \Delta\eta(\mathbf{r})\right]\cdot\nabla. \tag{2.7}$$

The fundamental modes of the perfect crystal are eigenmodes of $\hat{O}_0$,

$$\hat{O}_0\, H_{l,\mathbf{k}}(\mathbf{r}) = \lambda_{l,\mathbf{k}}\, H_{l,\mathbf{k}}(\mathbf{r}), \tag{2.8}$$

where l is the band index. $H_{l,k}$ are Bloch waves and can be written as

$$H_{l,\mathbf{k}}(\mathbf{r}) = \frac{1}{L} h_{l,\mathbf{k}}(\mathbf{r}) e^{i\mathbf{k}\cdot\mathbf{r}}, \qquad (2.9)$$

The Bloch modes near the degenerate satellite extrema of a band edge, which most strongly coupled together, are used to form the defect modes:

$$H_{d}(\mathbf{r}) = \sum_{i} c_{i} \sum_{\mathbf{k}} \tilde{\Gamma}_{i}(\mathbf{k} - \mathbf{k}_{i}) \frac{1}{L} h_{l,\mathbf{k}} e^{i\mathbf{k}\cdot\mathbf{r}}. \qquad (2.10)$$

where $\tilde{\Gamma}_i$ here are a set of envelope functions in the Fourier space, which in the spirit of the effective mass theory, have amplitudes locally around the satellite extreme points, k_i. See the illustration of the reciprocal space of the triangular lattice in Fig. 5.
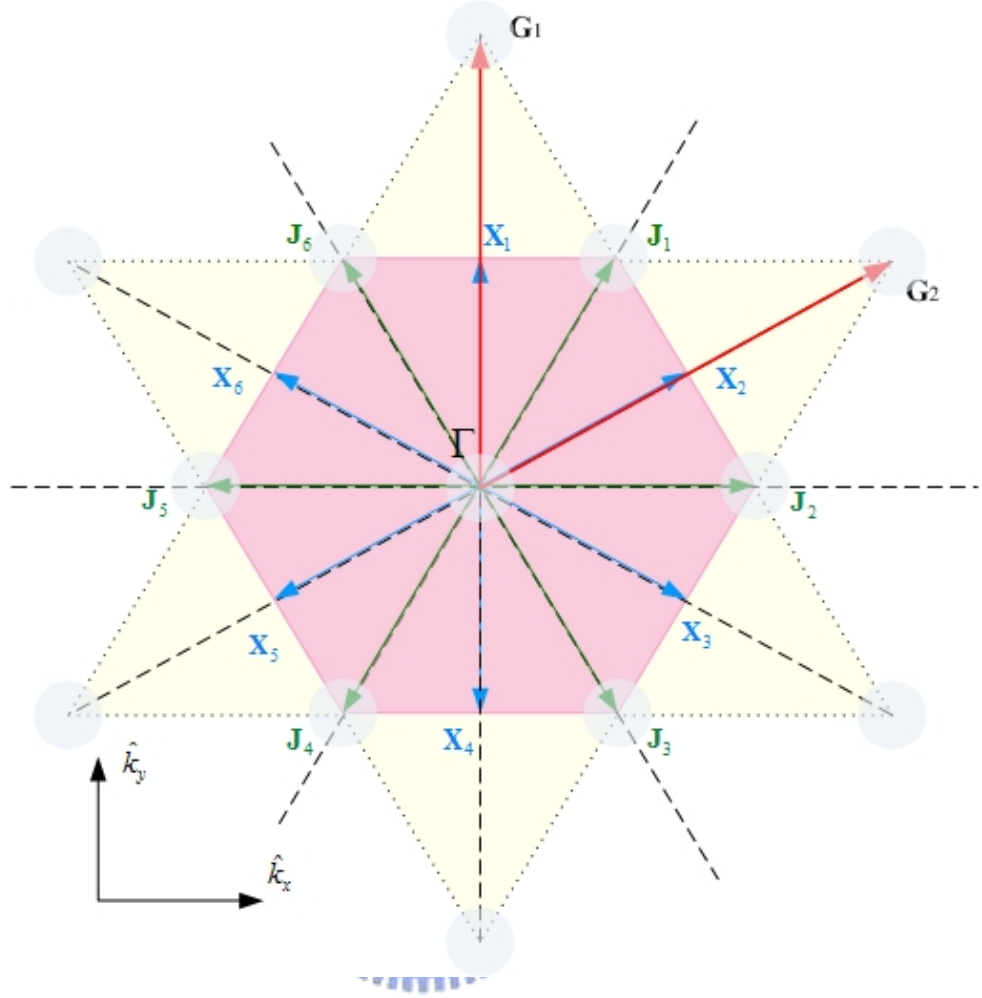
FIG 5 Illustration of the reciprocal spaces of the 2D triangular PC ($|G_1|=|G_2|=4\pi/\sqrt{3}a$, $|\mathbf{k}_X|=2\pi/\sqrt{3}a$, $|\mathbf{k}_J|=4\pi/3a$).

Representations of the mirror symmetry are shown.

Note that there is no inter-band mixing and neither is the band edge of interest degenerate.

Transforming the envelope functions into the real space make the defect modes become:

$$H_d(\mathbf{r}) \approx \sum_i c_i \frac{1}{L} h_{l,\mathbf{k}_i} e^{i\mathbf{k}_i \cdot \mathbf{r}} \Gamma_i(\mathbf{r}). \tag{2.11}$$

which can be viewed a result of the intra-band mixing of the unperturbed Bloch modes of the crystal.

To find an eigenvalue equation for the envelope functions, so return to Eq. (2.5):

$$\sum_j c_j \sum_{\mathbf{k}} \tilde{\Gamma}_j(\mathbf{k} - \mathbf{k}_j) \left\langle H_{l',\mathbf{k}'} \left| (\lambda_d - \lambda_{l,\mathbf{k}} - \hat{O}') \right| H_{l,\mathbf{k}} \right\rangle = 0. \tag{2.12}$$

With the assumption of only keeping the terms that mix states within the lth band, the strongest mixing terms is those states with k near the origin.

A further simplification can be made since the defect perturbations localized in k-space, and with this approximation,

$$\lambda_{\lambda,\mathbf{k}'} \approx \left[\lambda_{l,0} + \lambda_{\lambda,t}(\Delta\mathbf{k}) \right] + O(\Delta\mathbf{k}^3). \tag{2.13}$$

An approximate master equation for the localized magnetic field envelope functions of defect states in Fourier space representation is found.

Transform back to real space results in a set of coupled Wannier-like equations,

$$c_i \left\{ \left[\Delta\lambda_d - \lambda'_{l,i}\left(\hbar^{-1}\hat{\mathbf{p}}\right) \right] - \Delta\eta'_{l,i}(\mathbf{r}) \right\} \Gamma_\iota(\mathbf{r})$$

$$- \sum_{i \neq j} c_j \left[e^{-i\left(G_{j,i} - \Delta\mathbf{k}_{j,i}\right)\cdot\mathbf{r}} \Delta\eta'_{j,i}(\mathbf{r}) \right] \Gamma_j(\mathbf{r}) = 0, \qquad (2.14)$$

and an effective perturbation potential,

$$\Delta\eta'_{j,i}(\mathbf{r}) = \Delta\eta(\mathbf{r}) K_{l,l}\left[\left(\mathbf{k}_i, \mathbf{k}_j, \mathbf{G}_{j,i} \right) \right.$$

$$\left. + \nabla\left(\Delta\eta(\mathbf{r}) \right) \right] \cdot \mathbf{L}_{l,l}\left(\mathbf{k}_i, \mathbf{k}_j, \mathbf{G}_{j,i} \right). \qquad (2.15)$$

And further, the inter-k_i mixing as a perturbation to the envelope functions is formed from the local k-space mixing. This allows writing and independent Wannier-like equation for each of the $\Gamma_i(\mathbf{r})$ envelope functions,

$$\left\{ \left[\Delta\lambda_d - \lambda'_{l,i}(\hbar^{-1}\hat{\mathbf{p}}) \right] - \Delta\eta'_{i,i}(\mathbf{r}) \right\} \Gamma_i(\mathbf{r}) = 0. \qquad (2.16)$$

Of most importance for the types of resonant cavities studied here are the ground-state solutions to Eq. (2.16). For the present work, $\Gamma_i(\mathbf{r})$ is taken to be equal to the ground-state envelope, $\Gamma_{i,0}(\mathbf{r})$.

2.3   Donor defect mode around the X point

As a similar process in $\mathbf{k} \cdot \hat{\mathbf{p}}$ theory for Bloch electrons in crystalline materials, following two band magnetic field the eigenoperator is found as:

$$
\hat{O}_{X_i} = \begin{bmatrix} \tilde{\eta}_{0,\mathbf{0}}\left|\mathbf{k}_X\right|^2 & -\tilde{\eta}_{0,2\mathbf{k}_X}\left|\mathbf{k}_X\right|^2 \\ -\tilde{\eta}_{0,2\mathbf{k}_X}\left|\mathbf{k}_X\right|^2 & \tilde{\eta}_{0,\mathbf{0}}\left|\mathbf{k}_X\right|^2 \end{bmatrix}
\tag{2.17}
$$
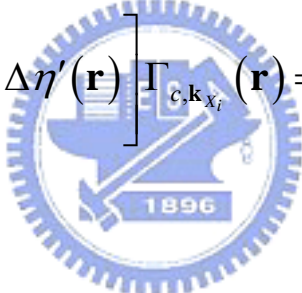
With the known, it's allowed to write for the local band structure of the conduction band in the vicinity of the Xi point,

$$
\lambda_{c,\mathbf{k}\sim\mathbf{k}_{X_i}} = \lambda_{c,\mathbf{k}_X} + \frac{\Delta\mathbf{k}_{x_i}^2}{m_{c,X,x_i}^*} + \frac{\Delta\mathbf{k}_{y_i}^2}{m_{c,X,y_i}^*}
\tag{2.18}
$$

with the effective "mass" defined as

$$\begin{cases} \dfrac{1}{m^*_{c,X,x_i}} = \tilde{\eta}_{0,\mathbf{0}}\left(1 - \dfrac{\tilde{\eta}_{0,2\mathbf{k}_X}}{\tilde{\eta}_{0,\mathbf{0}}}\right) \\[4ex] \dfrac{1}{m^*_{c,X,y_i}} = \tilde{\eta}_{0,\mathbf{0}}\left(1 - \dfrac{\tilde{\eta}_{0,2\mathbf{k}_X}}{\tilde{\eta}_{0,\mathbf{0}}} + \dfrac{2\tilde{\eta}_{0,\mathbf{0}}}{\tilde{\eta}_{0,2\mathbf{k}_X}}\right) \end{cases} \tag{2.19}$$

Lastly, for the Wannier equation of the conduction band envelope at the ith X point, it becomes

$$\left[\left(\dfrac{-\nabla^2_{x_i}}{m^*_{c,X,x_i}} + \dfrac{-\nabla^2_{y_i}}{m^*_{c,X,y_i}}\right) + \Delta\eta'(\mathbf{r})\right]\Gamma_{c,\mathbf{k}_{X_i}}(\mathbf{r}) = \left(\lambda_d - \lambda_{c,\mathbf{k}_X}\right)\Gamma_{c,\mathbf{k}_{X_i}}(\mathbf{r})$$

$$\tag{2.20}$$

2.4　　Formulation of problem

The case applicable to the above theory could be a defect cavity that results in an approximate harmonic perturbation potential. By appropriately varying the hole radii of the PC consisting of a triangular array of air holes in a host dielectric material, the inverse of the filling fraction of the triangular crystal can be graded in a roughly parabolic fashion, which is shown in Fig. 6:
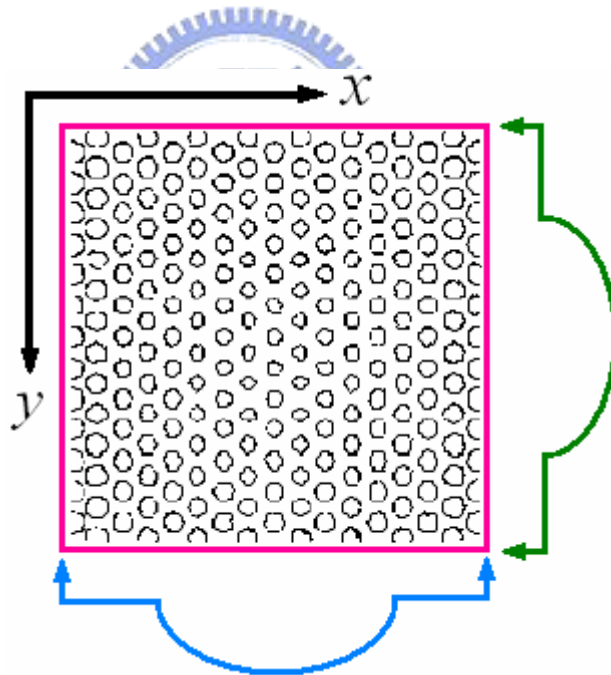

FIG 6　Illustration of the inverse filling fraction factor in a roughly parabolic harmonic fashion along x and y direction with green and blue lines are shown. In the center, a triangular lattice PC realizes with such air hole radii.

The filling fraction of the lattice, f, as a function of air hole radius is

$$f = 1 - \frac{2\pi}{\sqrt{3}} \left(\frac{r}{a} \right)^2,$$

(2.21)

For a host dielectric constant material of the refractive index n_0, the average dielectric constant of the patterned crystal is

$$\bar{\varepsilon} = f \left(n_0 \right)^2,$$

The resulting slowly varying envelope of the effective Wannier potential is

$$\Delta \bar{\eta}'_{i,i} (r) = \left| \mathbf{k}_X \right|^2 k \left(\frac{\rho}{a} \right)^2 \left(\frac{1}{n_0} \right)^2$$

$$= \left| \mathbf{k}_X \right|^2 k \left(\frac{x^2 + y^2}{a} \right)^2 \left(\frac{1}{n_0} \right)^2.$$

(2.22)

which is variable separable. Then, applying it to Eq. (2.20), then system is simplified into two one-dimensional cases, for its potential depends on x and y directions equivalently.

While only the different effective mass should be noticed, for the rest paragraph, just the case dependent on x is under consideration.

Now, following the theory metioned above, a hermitian operator is defined:

$$\hat{O}_{0,x} = \frac{\partial}{\partial x} \frac{-1}{m_x^*} \frac{\partial}{\partial x} + \Delta\eta'(x)$$

(2.23)

The subscript, '0', indicates the original system, compared to the system surrounded with the PML.

The total eigenvalue problem is then described as:

$$\hat{O}_{0,x}\Gamma_{x,n}^{(0)} = \lambda_x^{(0)}\Gamma_{x,n}^{(0)}$$

(2.24)

Assuming an infinite potential well covers the whole region of the PC medium, it's reasonable to define the basis functions as:
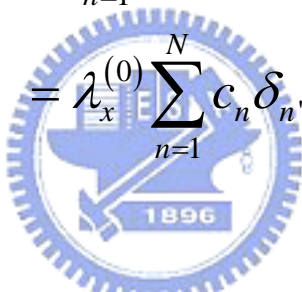
$$\Gamma_n^{(0)}(x) = \sum_{n=1}^{N} C_n \sqrt{\frac{2}{L_x}} \cos(\frac{n\pi}{L_x} x)$$

$$= \sum_{n=1}^{N} C_n \phi_n(x), \qquad n = 1,3,5....N$$

$$\Gamma_n^{(0)}(x) = \sum_{n=1}^{N} C_n \sqrt{\frac{2}{L_x}} \sin(\frac{n\pi}{L_x} x) \quad n = 2,4,6....N$$

(2.25)

The sets of even basis functions and odd basis functions form complete solutions for the hermitian operator.

The orthonormal relation is obeyed,

$$\left\langle \phi_{x,n'}^{(0)} \middle| \phi_{x,n}^{(0)} \right\rangle_{Lx} = \delta_{n',n} \tag{2.26}$$

Finally, solving this eigenvalue problem, the expanding coefficients, c_n, and

the eigenvalue, $\lambda_x^{(0)}$, can be found simultaneously:

$$\left\langle \phi_{x,n'}^{(0)} \middle| \hat{O}_{0,x} \middle| \Gamma_{x,n}^{(0)} \right\rangle_{Lx} = \sum_{n=1}^{N} c_n \phi_{x,n'}^{(0)}(x) \lambda_x^{(0)} \phi_{x,n}^{(0)}(x)$$

$$= \lambda_x^{(0)} \sum_{n=1}^{N} c_n \delta_{n',n} \tag{2.27}$$

And the envelope functions are obtained by expanding with the coefficients

and the even or odd basis functions.

3.   Perfectly matched layer

3.1   The split-field formulation of PML and the stretched PML

For aforementioned challenges of the efficient and accurate solution of electromagnetic wave interaction problems in unbounded regions, a desire of introducing the absorbing boundary condition (ABC) at the outer lattice boundary to simulate the extension of the wave solution to infinity is urgent. Since 1994, a new fervor in this area has been created by J. P. Berenger's introduction of a highly effective absorbing material ABC designated the PML [11]. The innovation of Berenger's PML is that plane waves of arbitrary incidence, polarization, and frequency can be matched at the boundary. To this end, Berenger derived a split-field formulation of Maxwell's equations.

Each vector field component is split into two orthogonal components. That is, in the continuous space, the PML absorber and the host medium are perfectly matched. By choosing loss parameters consistent with a dispersionless medium, a perfectly matched planar interface is derived.

The resulting modified curl equations in the time-dependent form can be depicted as [17]:

$$\left(\varepsilon_0\varepsilon_r\,\tfrac{\partial}{\partial t}+\sigma_y\varepsilon_r\right)E_{xy}=\tfrac{\partial}{\partial y}\left(H_{zx}+H_{zy}\right)$$

$$\left(\varepsilon_0\varepsilon_r\,\tfrac{\partial}{\partial t}+\sigma_z\varepsilon_r\right)E_{xz}=-\tfrac{\partial}{\partial z}\left(H_{yx}+H_{yz}\right)$$

$$\left(\varepsilon_0\varepsilon_r\,\tfrac{\partial}{\partial t}+\sigma_z\varepsilon_r\right)E_{yz}=\tfrac{\partial}{\partial z}\left(H_{xy}+H_{xz}\right)$$

$$\left(\varepsilon_0\varepsilon_r\,\tfrac{\partial}{\partial t}+\sigma_x\varepsilon_r\right)E_{yx}=-\tfrac{\partial}{\partial x}\left(H_{zx}+H_{zy}\right)$$

$$\left(\varepsilon_0\varepsilon_r\,\tfrac{\partial}{\partial t}+\sigma_x\varepsilon_r\right)E_{zx}=\tfrac{\partial}{\partial x}\left(H_{yx}+H_{yz}\right)$$

$$\left(\varepsilon_0\varepsilon_r\,\tfrac{\partial}{\partial t}+\sigma_y\varepsilon_r\right)E_{zy}=-\tfrac{\partial}{\partial y}\left(H_{xy}+H_{xz}\right)$$

(3.1)

Many papers appeared are validating Berenger's seminal work as well as applying the FDTD (the finite difference method in the time domain) with the PML medium. A number of modifications of the PML were also proposed to enhance its performance. And, the original split-field PML concept has also been restated in a stretched-coordinate form, which has been adopted and will be discussed in next section.

A much more compact form of the split-field equations was introduced by Chew and Weedon [3] and independently by Rappaport [12]. Here, the

split-field equations are re-posed in a nonsplit form that maps Maxwell's equations into a complex coordinate space. For the reason, a coordinate mapping into a complex space is introduced:

$$\tilde{x} \to \int_0^x s_x(x')dx', \quad \tilde{y} \to \int_0^y s_y(y')dy', \quad \tilde{z} \to \int_0^z s_z(z')dz' \qquad (3.2)$$

The stretched factors appear

$$\frac{\partial}{\partial \tilde{x}} = \frac{1}{s_x}\frac{\partial}{\partial x}, \quad \frac{\partial}{\partial \tilde{y}} = \frac{1}{s_y}\frac{\partial}{\partial y}, \quad \frac{\partial}{\partial \tilde{z}} = \frac{1}{s_z}\frac{\partial}{\partial z} \qquad (3.3)$$

The stretched gradient operator has the form:

$$\tilde{\nabla} = \hat{x}\frac{\partial}{\partial \tilde{x}} + \hat{y}\frac{\partial}{\partial \tilde{y}} + \hat{z}\frac{\partial}{\partial \tilde{z}} \qquad (3.4)$$

Maxwell's equations in the complex—coordinate stretched space are then expressed as:

$$i\omega\varepsilon\mathbf{E} = \tilde{\nabla} \times \mathbf{H}$$

$$= \hat{x}(\frac{1}{s_y}\frac{\partial}{\partial y}H_z - \frac{1}{s_z}\frac{\partial}{\partial z}H_y)+$$

$$\hat{y}(\frac{1}{s_z}\frac{\partial}{\partial z}H_x - \frac{1}{s_x}\frac{\partial}{\partial x}H_z)+ \qquad (3.5)$$

$$\hat{z}(\frac{1}{s_x}\frac{\partial}{\partial x}H_y - \frac{1}{s_y}\frac{\partial}{\partial y}H_x),$$

$$-i\omega\mu\mathbf{H} = \tilde{\nabla} \times \mathbf{E}$$

$$= \hat{x}(\frac{1}{s_y}\frac{\partial}{\partial y}E_z - \frac{1}{s_z}\frac{\partial}{\partial z}E_y)+$$

$$\hat{y}(\frac{1}{s_z}\frac{\partial}{\partial z}E_x - \frac{1}{s_x}\frac{\partial}{\partial x}E_z)+ \qquad (3.6)$$

$$\hat{z}(\frac{1}{s_x}\frac{\partial}{\partial x}E_y - \frac{1}{s_y}\frac{\partial}{\partial y}E_x).$$

With some approximations, one familiar 2D case is that Eq. (3.5) and Eq. (3.6) can be coupled to make a wave equation, what will be a similar form with the forthcoming equation, Eq. (3.9).

3.2   Envelope function with the PML
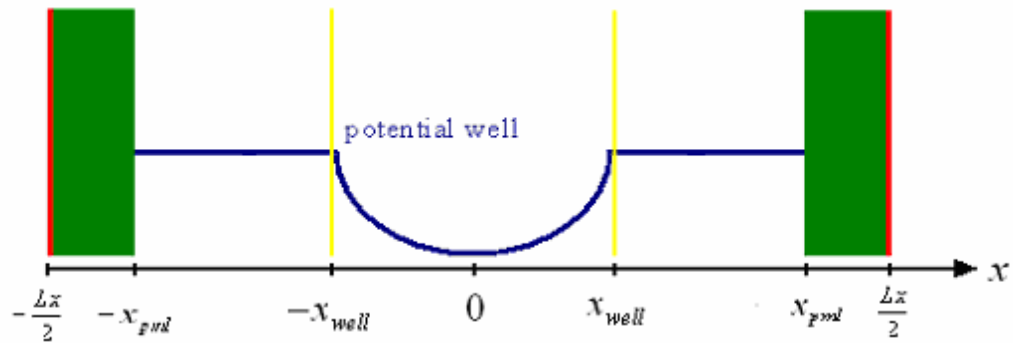
FIG 7   Illustration of the nomenclature for the positions along the x axis. The green region is the PML.

The red line depicts an infinite potential well at the rim of this system.

Considering the one-dimensional case, the graded-filled PC results in a parabolic form of the inverse dielectric constant distribution. For this case, it emerged as the effective Wannier potential term, $\Delta\eta'(x)$, in Eq. (2.23). Depicting $\Delta\eta'(x)$ along the x-axis in this system, (also see Fig. 7)

$$\Delta\eta'(x) = \begin{cases} \left|\mathbf{k}_x\right|^2 \dfrac{k}{n_0^2} x^2 & -x_{well} < x < x_{well} \\[4mm] \left|\mathbf{k}_x\right|^2 \dfrac{k}{n_0^2} x_{well}^2 & -x_{well} > x, \; x < x_{well} \end{cases} \qquad (3.7)$$

And, the Eq. (2.23) can be reformed as:

$$\left(\frac{\partial}{\partial x} \frac{-1}{m_x^*} \frac{\partial}{\partial x} + \Delta\eta'(x) \right) \Gamma_x(x) = \lambda_x \Gamma_x(x) \qquad (3.8)$$

The eigenfunction $\Gamma_x(x)$ in the above equation described the envelope function of the localized modes confined by the parabolic potential well. The first several modes, i.e. bound state, is well confined in the potential well, while some modes with higher eigen-frequency leak out the well and travel through the constant potential region. After leaking out the potential well, the modes was subjected unchanged potential, the sovereign equation under this situation thus became

$$\left(\frac{\partial}{\partial x} \frac{-1}{m_x^*} \frac{\partial}{\partial x} + \Delta\eta'(x_{well}) \right) \Gamma_x(x) = \lambda_x \Gamma_x(x) \qquad (3.9)$$

As a result, the reasonable solution for this equation is plane waves, and a PML-applicable condition appears.

To investigate these leakage modes evanescent into infinity, the PML surrounded the PC medium is introduced, which applied with the concept of stretched PML medium and modified the Eq. (3.9) like:

$$\left(\frac{1}{s_x} \frac{\partial}{\partial x} \frac{-1}{m_x^*} \frac{1}{s_x} \frac{\partial}{\partial x} + \Delta \eta'(x) \right) \Gamma_x(x) = \lambda_x \Gamma_x(x),$$ (3.10)

where the S_x is the complex stretched parameter, and its imaginary part , Sx, should be well determined to reach efficient convergence. The discussion about the magnitude and properties of Sx is presented in the next section.

In conclusion, when a leakage mode travels in normal medium or PML with the position-independent potential, it can be viewed as a plane wave:

$$-\frac{\partial^2}{\partial x^2} \Gamma_x(x) = m_x^* \left(\lambda_x - \Delta \eta'(x_{well}) \right) \Gamma_x(x),$$

$$-\frac{1}{S_x} \frac{\partial}{\partial x} \frac{1}{S_x} \frac{\partial}{\partial x} \Gamma_x(x) = m_x^* \left(\lambda_x - \Delta \eta'(x_{well}) \right) \Gamma_x(x).$$ (3.11)

If these two equations were solved by

$$\Gamma_x(x) = \exp(-ik_{nor}x),$$

and

$$\Gamma_x(x) = \exp(-ik_{pml}x),$$

29

respectively. It would be found

$$k_{nor} = \sqrt{m_x^* \left(\lambda_x - \triangle \eta' \left(x_{well} \right) \right)}.$$ (3.12)

Then,

$$k_{pml} = S_x k_{nor}.$$ (3.13)

3.3   Determination of the stretched parameter

In this section, it is to find out the value and dependent properties of the stretched parameter for the PML layer in this system. Only under consideration is the one-dimensional planar PML medium, which is as the one shown in Fig. 7.
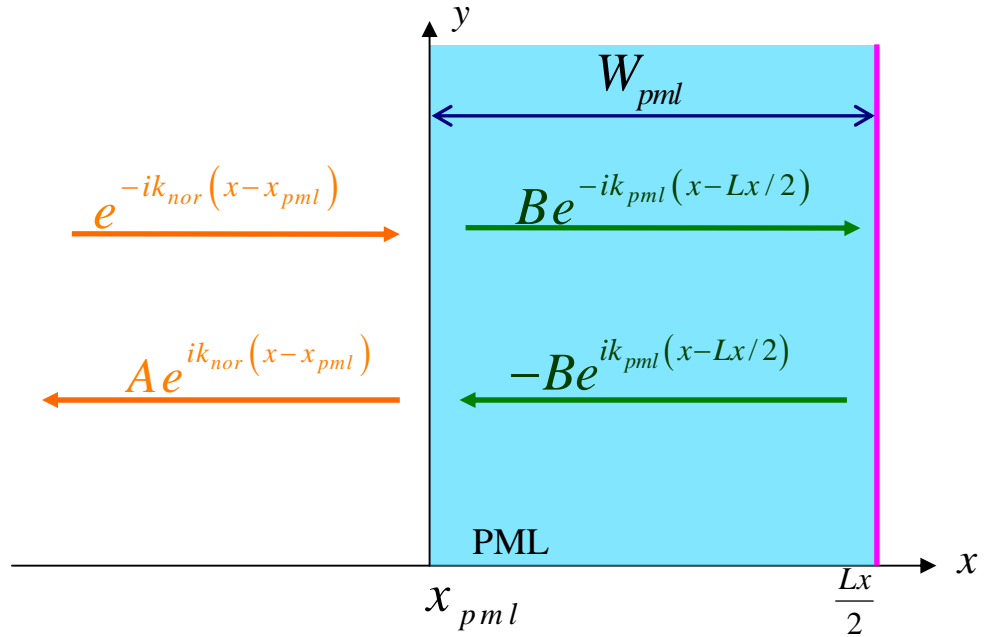
FIG 8   The plot for field travels in the form of plane waves through the interface between the normal

medium and the PML.

By Fig. 8, when a plane wave incident through the interface between the normal medium and the planar PML medium in the x direction, one transmitted wave and one reflective wave take place. After passing through the PML medium, the transmitted wave was totally reflected by the artificial interface (plotted by pink line at $x = Lx/2$). And, introducing the non-reflection boundary condition for the total fields located at both sides of the PML interface is the next step. That is, they were made equal:

$$e^{-ik_{nor}(x-x_{pml})} + Ae^{ik_{nor}(x-x_{pml})} = Be^{-ik_{pml}(x-Lx/2)} - Be^{ik_{pml}(x-Lx/2)} \qquad (3.14)$$

And, the amplitude of the reflective wave can be represented as:

$$A = -e^{ik_{pml} \cdot 2W_{pml}},$$

By the relation in Eq. (3.13),

$$A = -e^{iSk_{nor} \cdot 2W_{pml}},$$

The reflectivity at the PML interface is

$$R = |A|^2 = e^{-2k_{nor}Sx \cdot 2W_{pml}} \ll 1 \qquad (3.15)$$

where the stretched parameter

$$S_x = 1 + iSx. \qquad (3.16)$$

So, here is an approximation that the envelopefunction evanescence at $x = Lx/2$. The reflectivity in this system was made as samll as $\exp(-8)$.

Observing the Eq. (3.15), the dimension of the imaginary part of the stretched parameter depends on the effective mass and the thickness of the

PML layer. In the Table 1, some S values (imaginary part only) on different PML thicknesses along two different directions are shown.

Sx	Wpml =5(a)	Wpml =13(a)	Sy	Wpml =5(a)	Wpml =13(a)
Sx,1	-2.1432	-1.6123	Sy,1	-3.0403	-2.8766
Sx,2	-1.1711	-0.4804	Sy,2	-1.4293	-1.5718
Sx,3	-0.8280	-0.3218	Sy,3	-1.0624	-1.1113

Table 1   Some calculated imaginary part of the stretched parameter for different width of the PML and the different direction, x and y.

However, since the acceptable range of choosing approximate zero at the rim of the system, what really matters is the dimension, not the accurate value of S. The negative sign is reasonable for the planewave field proportional to harmonic time part, $e^{i\omega t}$, decaying with increasing distance in the PML.

3.4　　Formulation of problem

For the system surrounded the PML, a new eigenoperator:

$$\hat{O}' = \frac{1}{s_x}\frac{\partial}{\partial x}\frac{-1}{m_x^*}\frac{1}{s_x}\frac{\partial}{\partial x} + {}_{\vartriangle}\eta'(x).$$

(3.19)

Here, the same notation following Chew's stretched parameter, s_x, is used.
And expanded it with the orthonomal functions, sine and cosine, i.e., the basis functions in the system without the PML,

$$\hat{O}'_x\Gamma^{(0)}_{x,n}(x) = \lambda_x\Gamma^{(0)}_{x,n}(x).$$

(3.20)

Then, following the same procedure described in the section 2.4, diagonalizing this nonhermitian matrix,

$$\left\langle \phi^{(0)}_{x,n'}\left|\hat{O}'\right|\Gamma^{(0)}_{x,n}\right\rangle_{Lx}$$

(3.21)

can find the eigenvalue for the frequency of the defect states and the corresponding coefficients which can expand the envelope functions.

4. Simulation results

To investigate the effect of the PML layer and optimize the stretched parameter, some simulation results throughout this chapter perform. And some results of the original system without the absorbing medium are present to compare.

This chapter is divided into three sections. In the first section, the main topic is focusing on the bounded state with two different systems. One is the PC slab wave surrounding an infinite well, while another is placing the PML into the medium. In the next section, the leaky modes of this system with the aid of the PML are found and signified by the distribution of the envelope function. The third section shows the calculated defect mode frequencies.

4.1 Photonic band-gap for 2D triangular lattice

The plane-wave expansion method [18] was used here to calculate the photonic band-gap and obtain the photonic band structure for this system. Fig.2 and Fig.9 differ in their average relative permittivities of each unit cell, which are ε_i and ε_f, respectively. The parabolically changed drilling radius of air holes results in different average permittivities. The ratios of the radii to the conventional lattice constant, r/a, are 0.380 and 0.400, respectively. What should be noticed is that 0.380, $(r/a)_0$, it determines the unperturbed parameter in my PC system. Following the effective index method for the z-direction optical guiding, the refractive index n_0 is 2.650 for this quasi 2D system. In addition, to obtain this figure, the number of plane waves used is more than 1000. Further, the line with yellow color specifies the location of light-line in the normalized photonic band-gap structure. Finally, the gray sections locate the absolute gap for TE modes in 2D triangular PC lattice under these conditions.

Besides, this method is utilized to determine the magnitude of $\lambda_{c,\mathbf{k_x}}$, which is the square value of the conduction band edge.
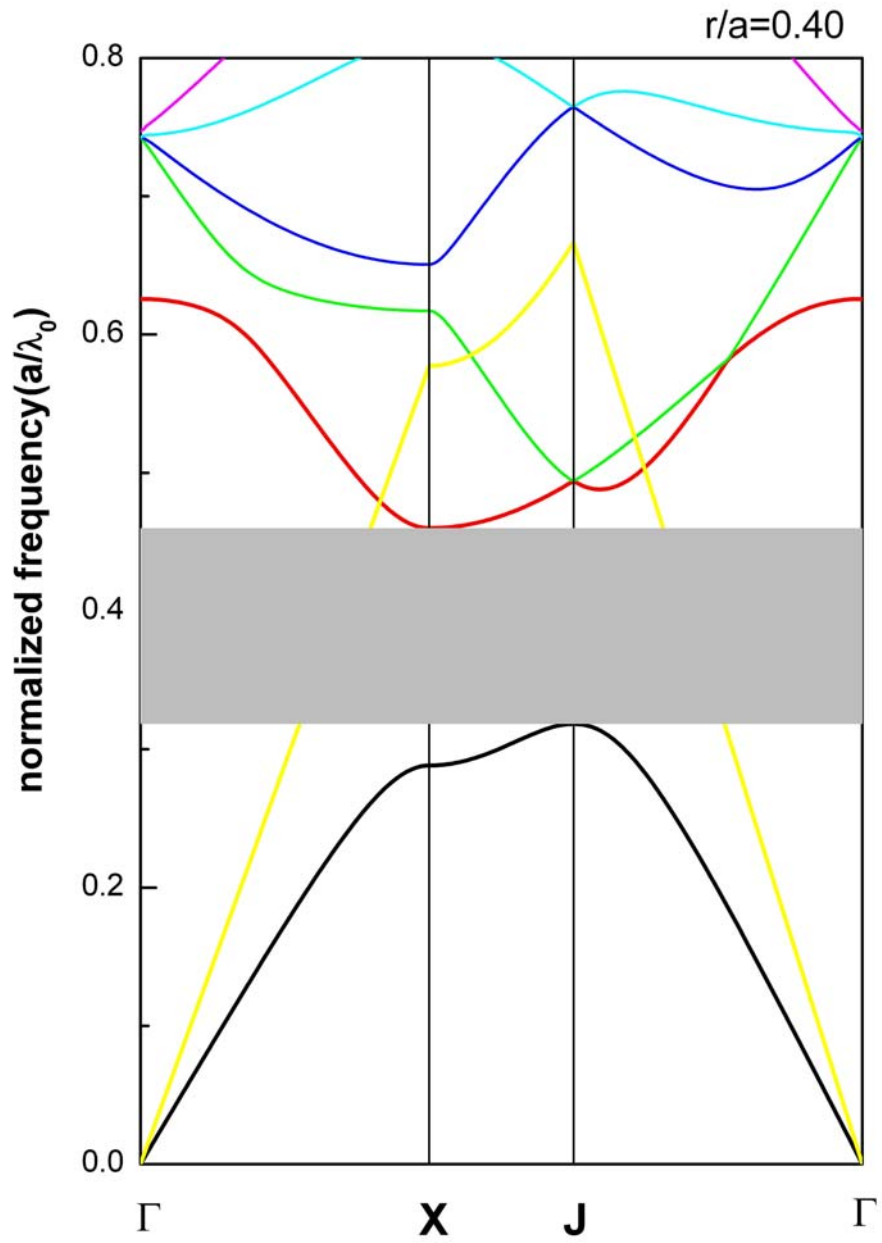
FIG 9   The fundamental TE-like guided mode band structure (r/a=0.380, $n_{eff} = n_{slab} = 2.650$).

	r/a	CB Edge $(\omega a/\lambda_0)$	VB Edge $(\omega a/\lambda_0)$	Bandgap $(\omega a/\lambda_0)$
Fig.2	0.3800	0.4337	0.3036	0.130
Fig.9	0.4000	0.4599	0.3184	0.142

Table 2   Some parameters and results for the photonic band structure by plane wave expansion method.
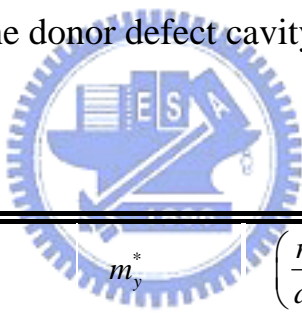
In the Table. 2, some important parameters used in simulating process are specified.

4.2 The envelope function for the defect mode — guided mode

In this section, the simulation results that plot the envelope functions of the guided defect modes in this graded-filled photonic crystal medium are demonstrated. Eq. (2.24) and Eq. (3.20) are followed by two different cases. Some parameters for the donor defect cavity are tabulated in Table.3.

m_x^*	m_y^*	$\left(\dfrac{r}{a}\right)_0$	$\left(\dfrac{r}{a}\right)_f$
2.2049	0.1811	0.38	0.40

x_{well} (a)	K	$\Delta\bar{\eta}'\left(x_{well}\right)$	N_0	N_{pml}
11.90	0.002	0.0134	600	800

Table 3   Some important parameters used to simulate are tabulated.

In Fig. 9, Fig. 10 and Fig. 11, guided modes estimated by the system without the PML, are found.

Fig.9 and Fig. 10 show the envelope functions expanded with the even and odd basis functions, respectively, which depict the guided modes (eigenvalues locate at states below the potential wall barrier) localized in the potential well. With the settings, there are about seven allowed guided states along x direction. The seventh state in Fig. 9 (e), that is, the highest guided mode has a long leaky tail into the potential barrier region. For efficient convergence of higher-order eigenvalues, and valid evanescence of envelope function at the edge, at least 100 basis (N_0) is needed.

Fig.11 performs the guided modes along y direction. For the "lighter" effective "mass", there are only two modes guided in the same potential well.

Simultaneously, by observing the eigenvalues, for a parabolically distributed potential well, almost equivalent distance between each neighboring state was found.

In all the figures of envelope functions, (a) picture plots the envelope function of the Wannier-like well potential in order to show the location of the finish of potential change.
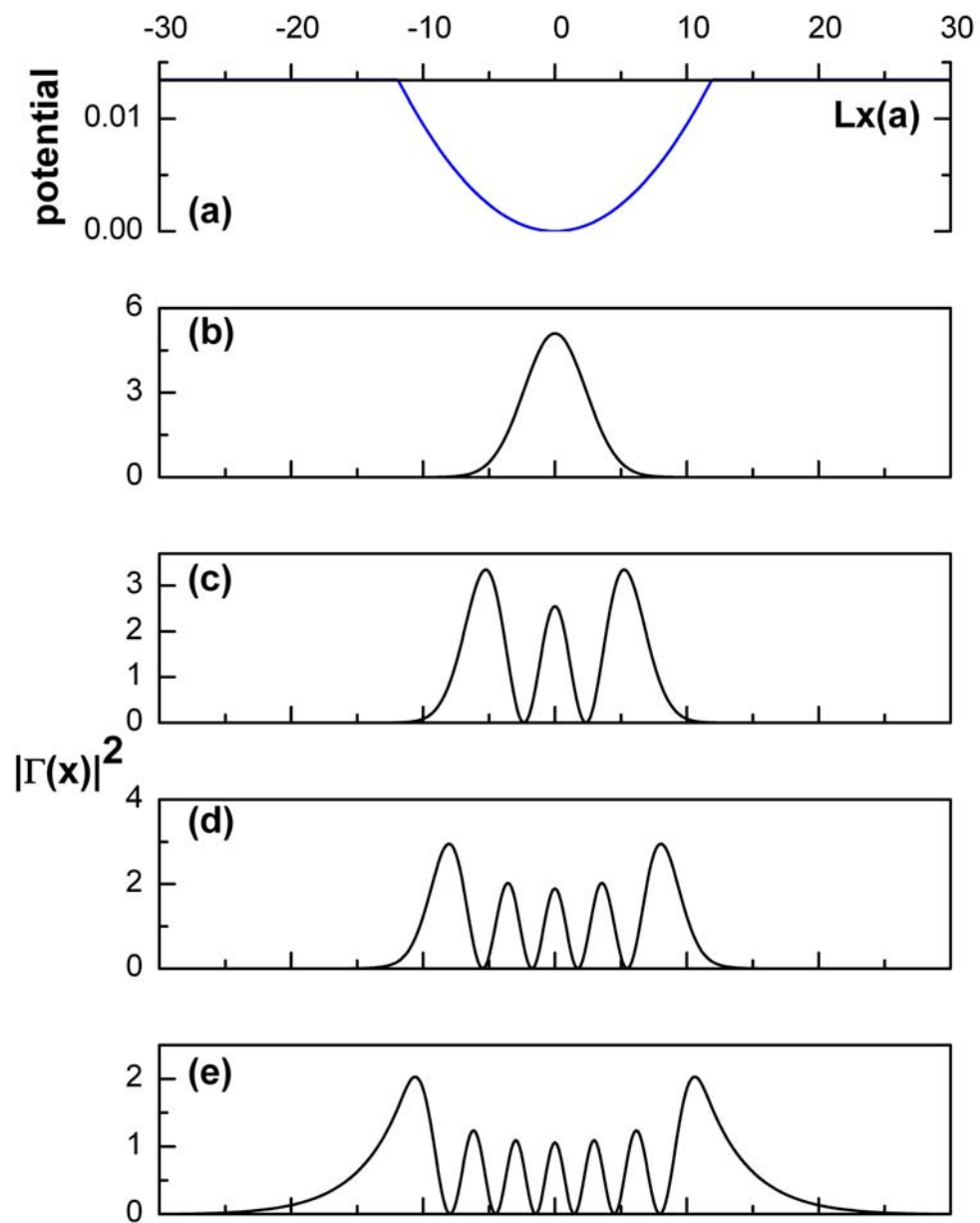
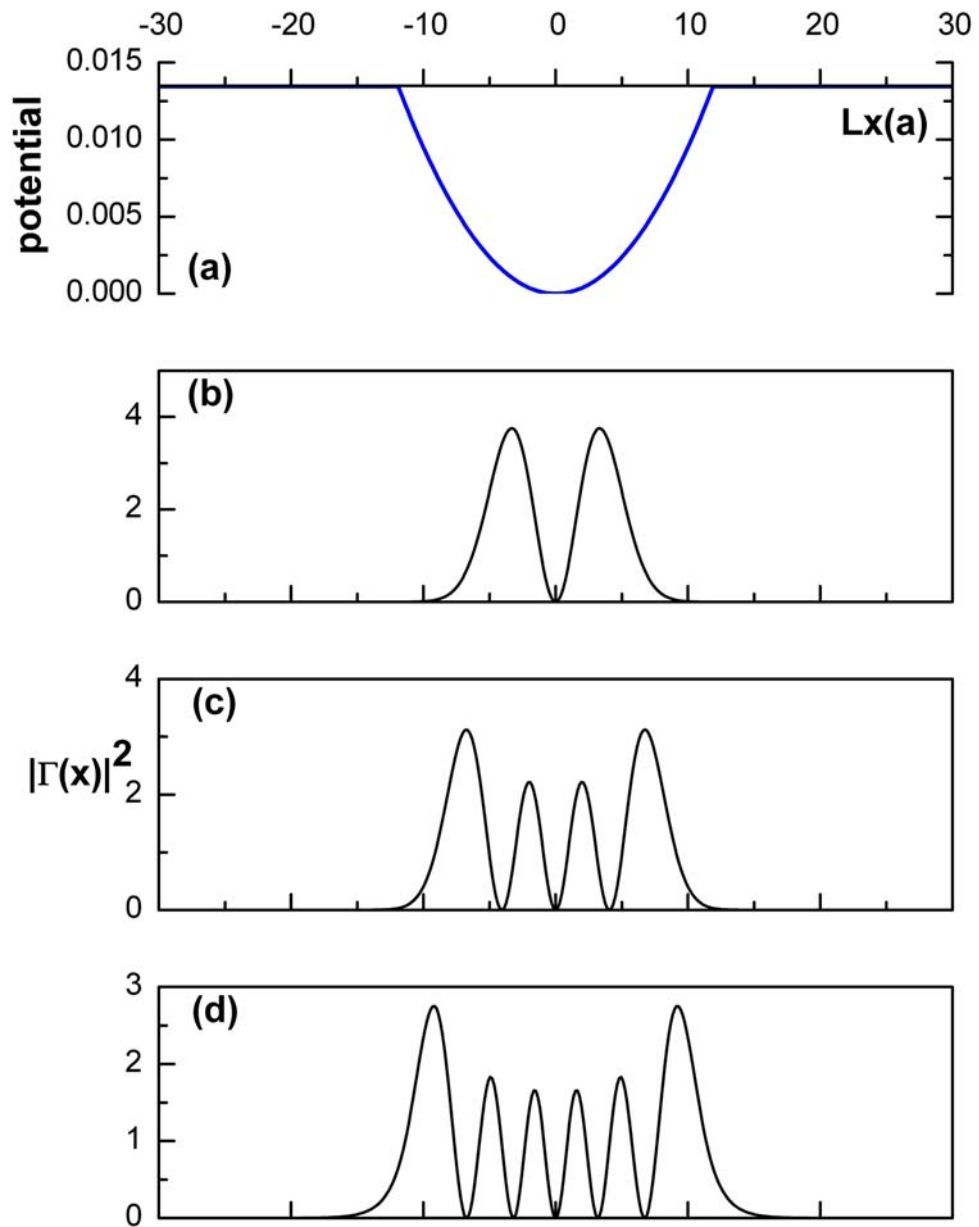FIG 10   The envelope functions of the guided even modes along x-direction. The total length is 60a.

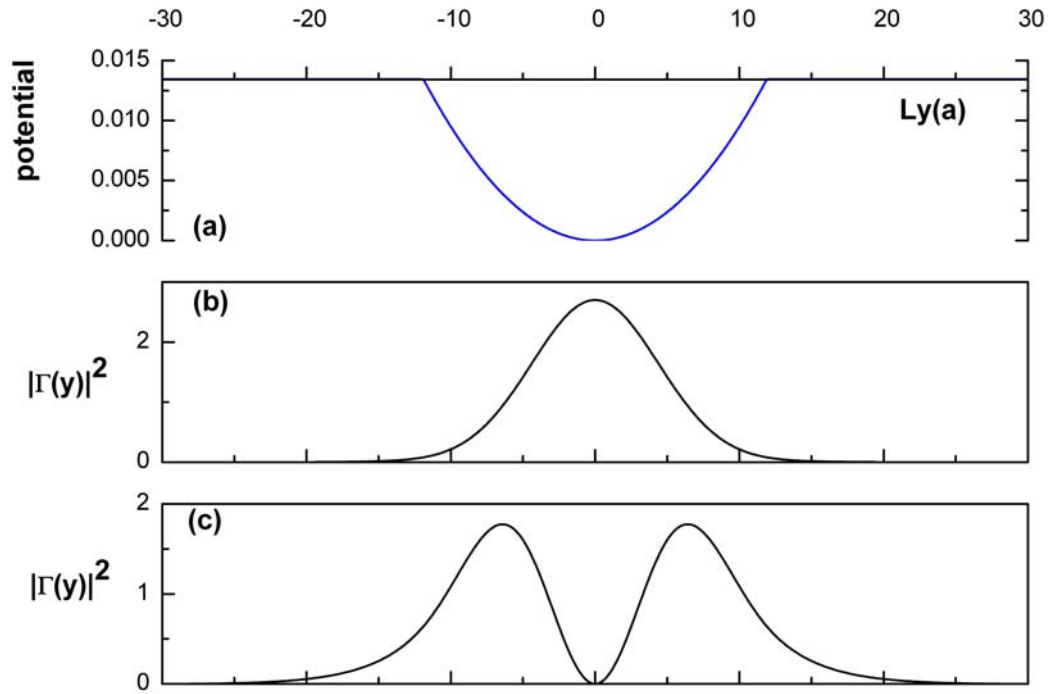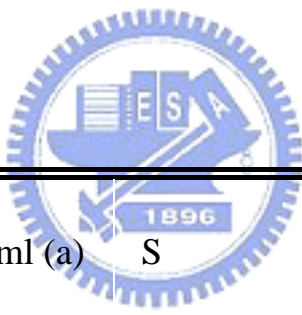FIG 11   The envelope functions of the guided odd modes along x-direction. The total length is 60a.

FIG 12   The envelope functions of the guided modes along y-direction. The total length is 60a.

To proceed, placing a layer of the absorbing medium, PML, can also reach similar simulation results of guided modes. In the Fig.13, the system with total length the same as the above case was be put the PML at the edge, whose thickness is 13 a (a means the conventional lattice constant). A similar profile of the envelope function is got and the difference of eigenvalues with the case without the PML is at the third figure after the decimal point. For comparison, there are 24 sets of systems with different thickness of the PML and different total length of the PC medium used.

L (a)	Wpml (a)	S	N
60	8	Sx	
60	13	=-2.1432	800
		Sy	
60	18	=-1.5718	

Table 4   Different parameters for calculating the envelope functions.

L (a)	Wpml (a)	S	N
	3	Sx	
	5	=-2.1432	
40		Sy	800
	8	=-1.5718	

Table 5   Different parameters for calculating the envelope functions.

The simulation results of each set of parameters meet well with the results in the case without the PML.
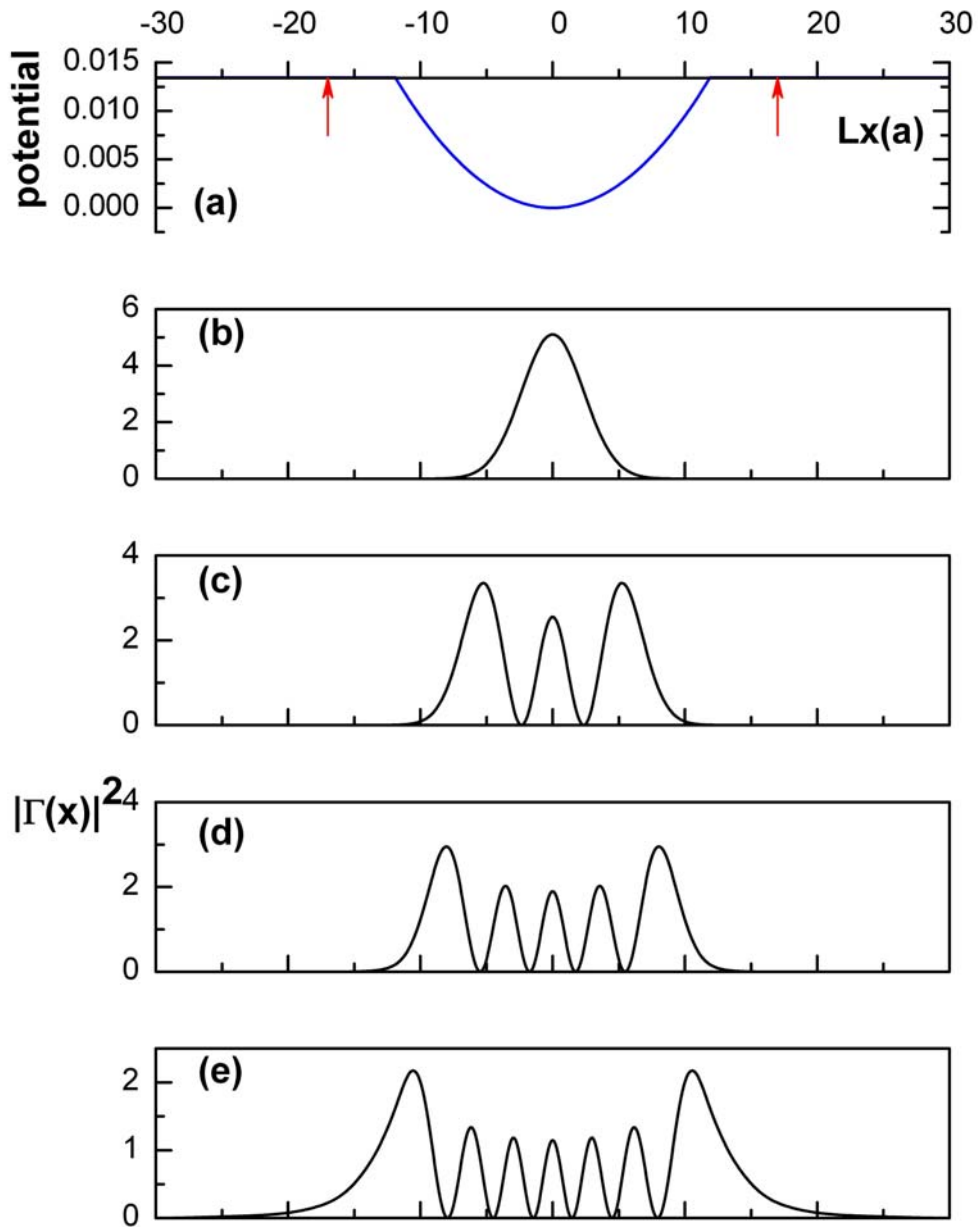
FIG 13 The envelope functions of the guided even modes along x-direction. Surrounding the PML with

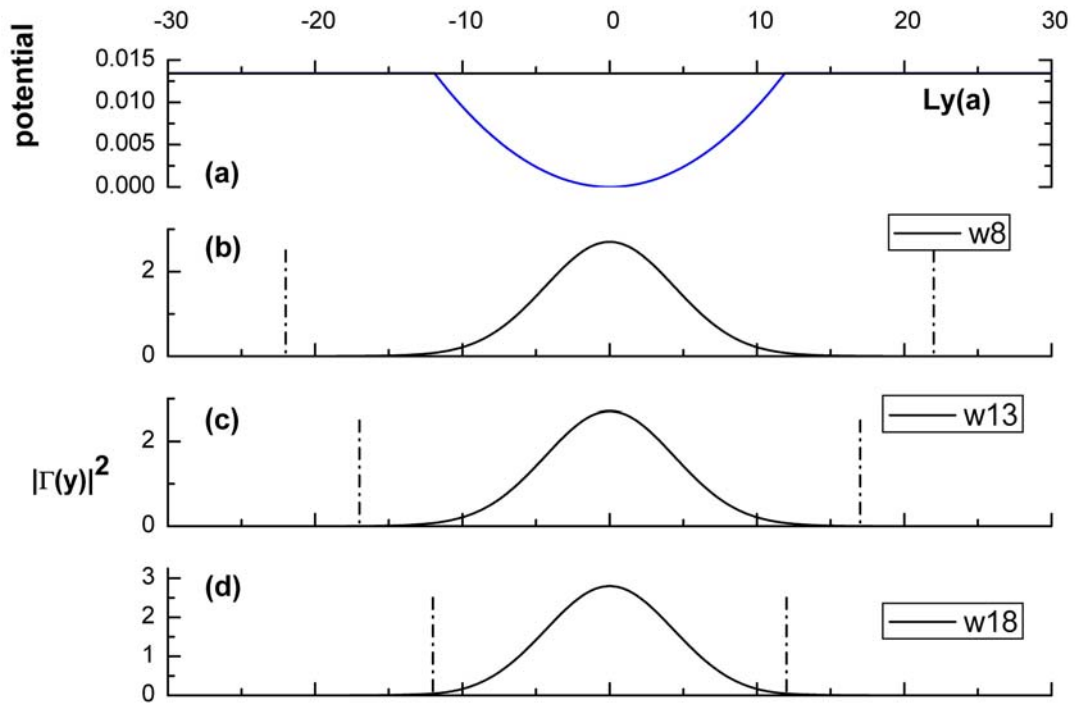thickness=13a. The total length is 60a.

FIG 14   The envelope functions of the first guided mode along y-direction. Surrounding the PML with

different thickness=8a, 13a 18a. The total length is 60a.

Fig. 14 is plotted to compare the effect of the thickness of the PML on the envelope function. The first guided modes for the y-direction eigenvalue equation are shown. Most importantly, when the thickness increases and reaches the well edge, unwanted truncation occurs, which results in a small dimension of inaccuracy at the magnitude of the eigenvalue. Besides, compared to the system without the PML, this system needs more basis functions in order to make sure the complex eigenvalues convergent well.

4.3   The envelope function for the defect

mode—leakage mode

Introducing the PML into the system, it's able to investigate the properties and distribution profile of the leaky modes. Some reasonable and reliable simulation results are shown.

Surrounded the PML layer, the leakage modes are computed with three different sets of parameters (see Table. 4) tunneling through the medium, where the Fig.15, Fig.16 and Fig. 17 depict the first four leakage modes for different settings. The arrow sign in each picture points out the position of the interface between the PC medium and the PML layer. As mentioned in chapter 3, the wave solutions here can be classified into two kinds [19]. One is the quasi-bounded states, what is wanted and have the form as (c), (d), (e), (f). There are also infinite radiation modes, which form as (b).

Examining the eigenvalues of these leaky modes, those for the radiation modes exist unexpectedly, while those for the quasi-bounded states appear with their magnitude in a reasonable periodic way. That is, near the bottom of the infinite square potential well, the difference of the eigenvalues of neighboring quasi-bound states is smaller.
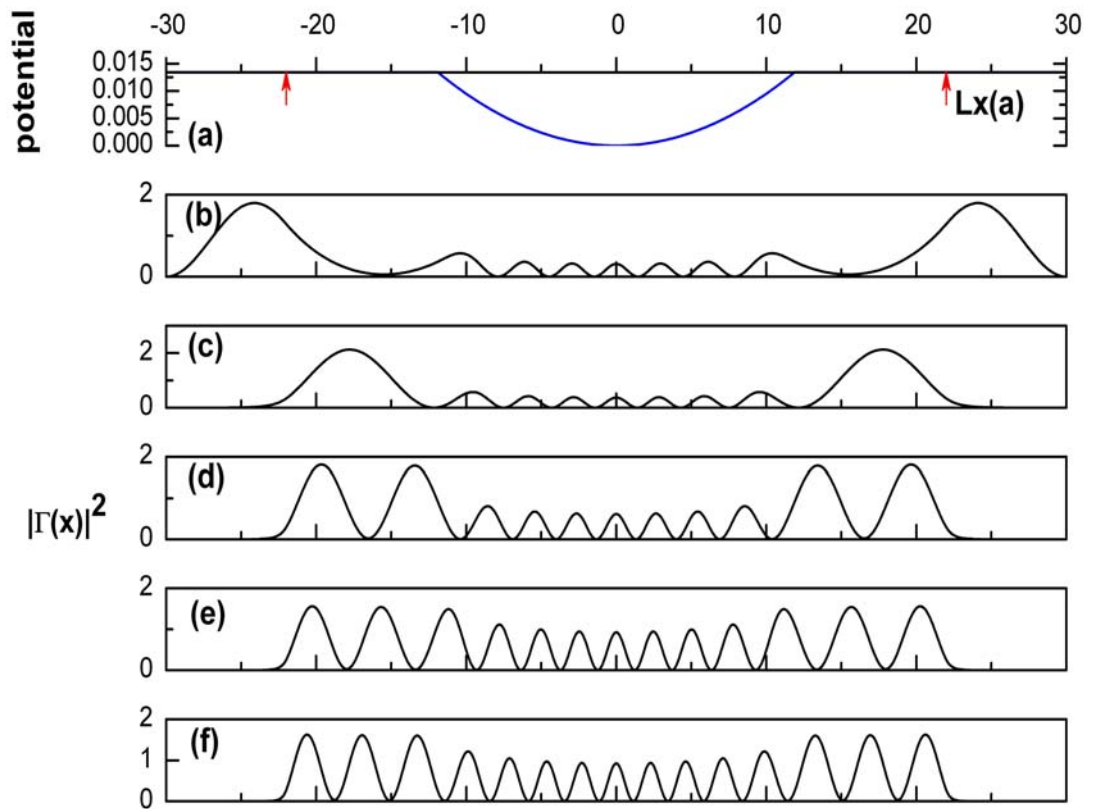
FIG 15 The envelope functions of the leaky even modes along x-direction. Surrounding the PML with thickness=8a. The total length is 60a.

FIG 16   The envelope functions of the leaky even modes along x-direction. Surrounding the PML with

thickness=13a. The total length is 60a.

FIG 17 The envelope functions of the leaky even modes along x-direction. Surrounding the PML with thickness=18a. The total length is 60a.

However, when focusing the (c), (d), (e), (f) in the Fig.15, Fig.16 and Fig.17, the distribution of the leaky modes is strongly affected by the width of the PML unlike the case for guided modes. The effect reflects on the eigenvalues as the increase with the larger width of the PML.
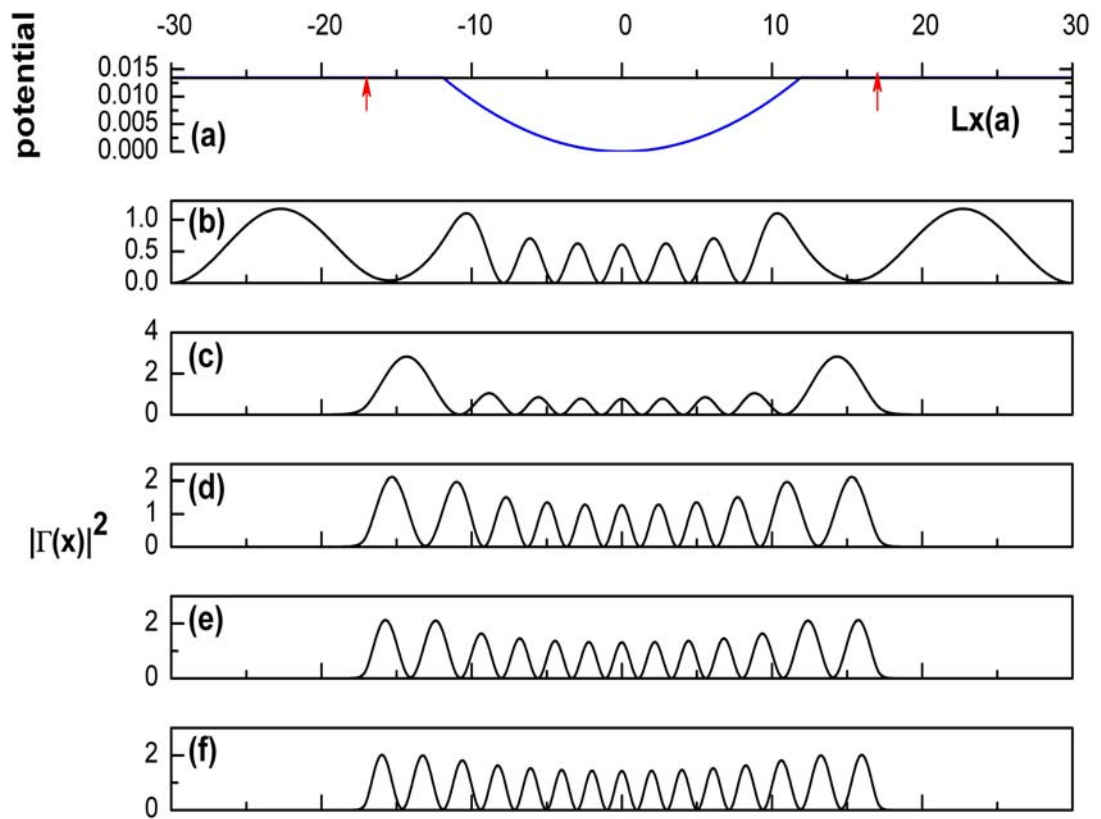
FIG 18   The envelope functions of the leaky even modes along y-direction. Surrounding the PML with thickness=13a. The total length is 60a.

Fig. 18 shows the leaky modes along the y-direction with the same total length. Along the y-direction, the third mode becomes leaky. Two similar profiles are obtained and appear in (e) and (f). They have similar profile and eigenvalues, but they are not totally the same.
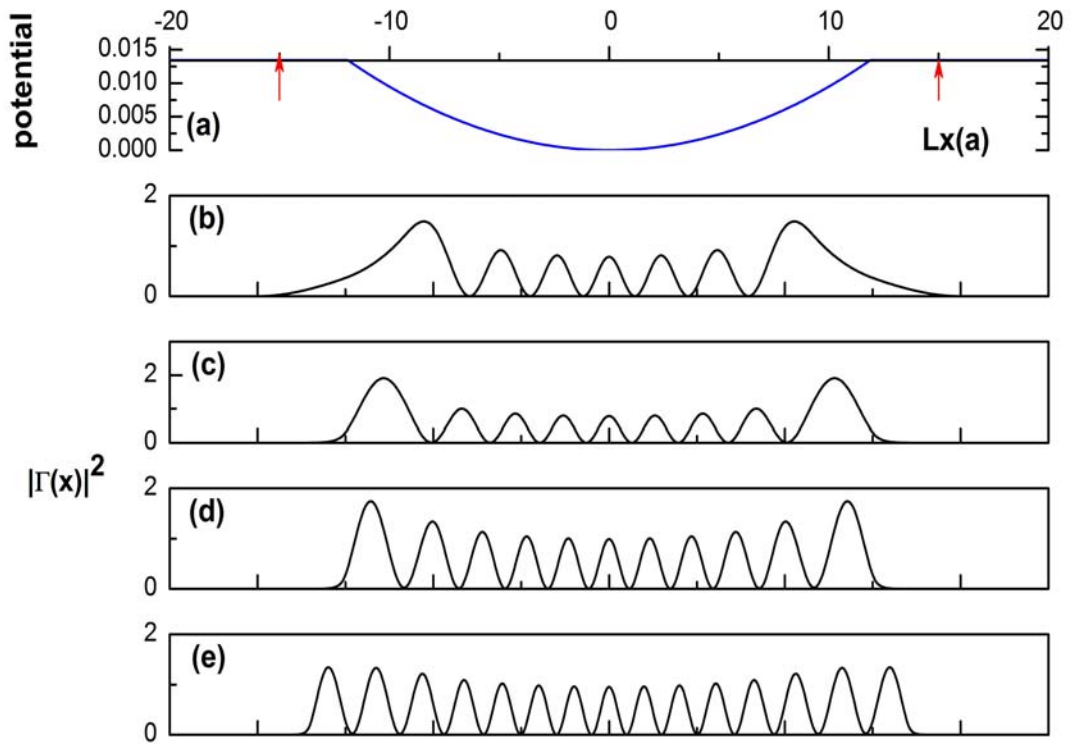
FIG 19   The envelope functions of the leaky even modes along y-direction. Surrounding the PML with
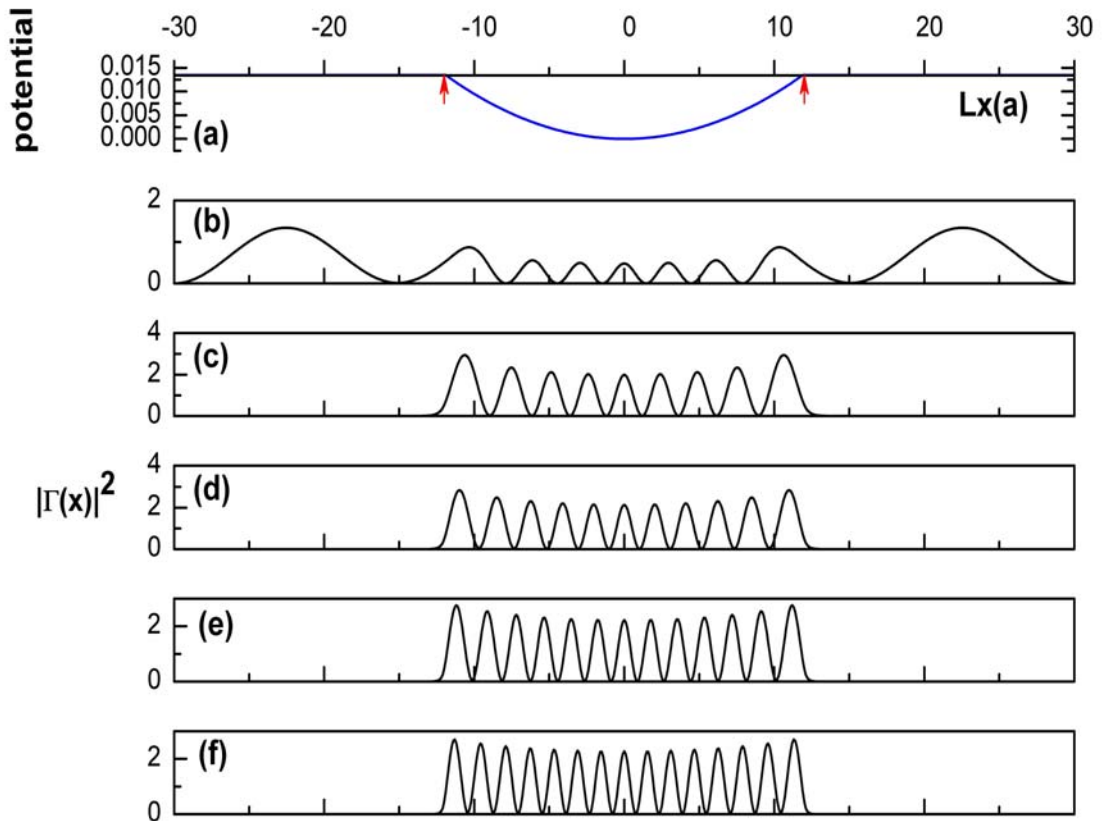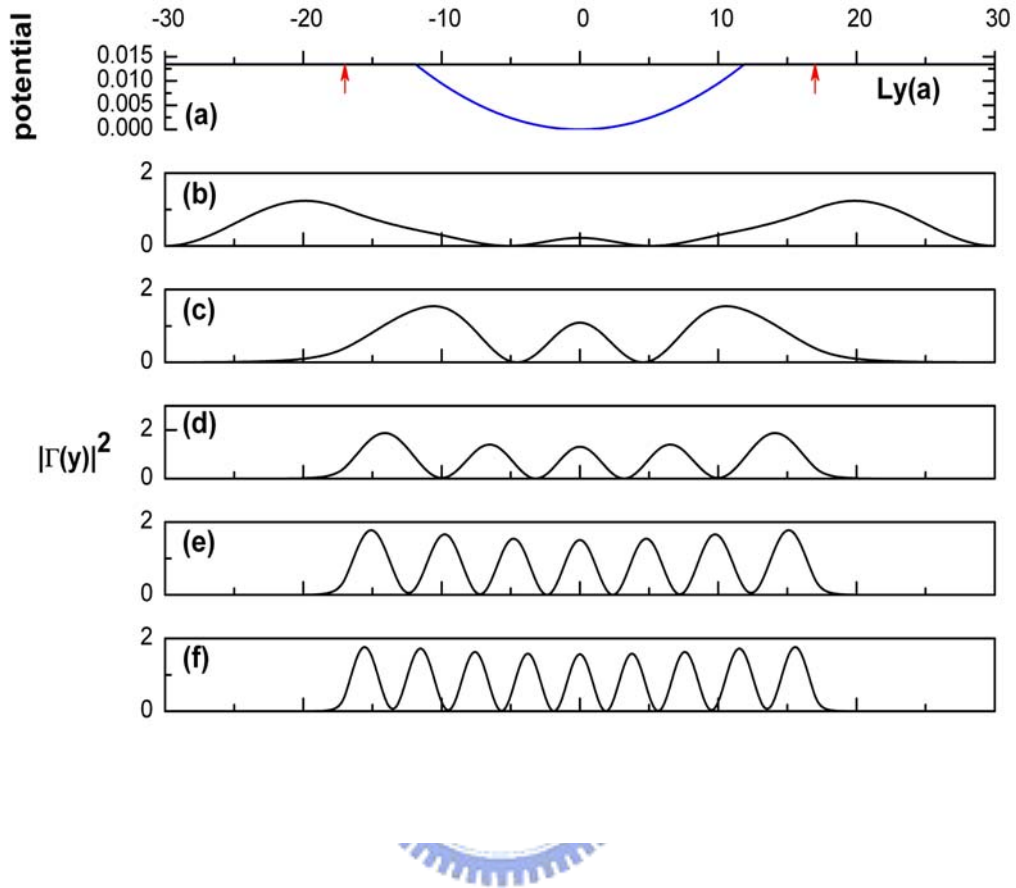
thickness=5a. The total length is 40a.

Decreasing the total length of the system, the efficiency to get the guasi-bounded states for the PML is increasing. The thinner of the potential well, the more unwanted radiation states disappear. In Fig. 18, (b) shows the last guided mode, which has a long tail into the barrier. The figures (c), (d), and (e) show the first three leaky even modes.

In summary, a suitable but shorter total length can improve the efficiency of

the PML. This also means less number of basis functions to reach convergence is needed. In addition, the system with the too thin PML, the magnitude of eigenvalues is unstable, especially for the higher modes, and the modes near the top of the potential well. However, the system with too thick PML close to the edge of the well, the tail of distribution of the field is forced to decay and the eigenvalue of the state is affected.

4.4　The defect frequency

In the last section, the defect frequencies for several above cases are present, and discuss their differences.

Firstly, the eigenvalues in Eq. (2.24) and Eq. (3.20) along x and y directions have been obtained. Following the Eq. (4.1), and coupling the results in first section of this chapter, it's easy to find the donor defect mode near the conduction band edge,

$$\lambda_d = \left(\lambda_x + \lambda_y\right) + \lambda_{c,\mathbf{k_x}}, \tag{4.1}$$

and so the normalized frequency is as

$$\omega_d = \sqrt{\lambda_d}.$$

Table 4 shows the eigenvalues in the case without PML. The defect frequency is real. Since this model is suitable for guide modes, the higher modes are expected to be inaccurate.

L=60	
1st	0.4234
2nd	0.4259
3rd	0.4283
4th	0.4307
5th	0.4314
6th	0.4331
7th	0.4338
8th	0.4362
9th	0.4366
10th	0.4386

Table 6   The defect modes frequency calculated by the original system.

Then, the case with the PML is under discussion. Table 7 shows the system with total length equal to 60a.

L= 60	Wpml=8		Wpml=13		Wpml=18	
	Real	Imaginary	Real	Imaginary	Real	Imaginary
1st	0.4234	1.0451E-7	0.4234	1.1865E-5	0.4235	1.6543E-4
2nd	0.4257	1.0220E-6	0.4258	1.5050E-5	0.4259	2.0003E-4
3rd	0.4283	1.0332E-6	0.4284	1.5084E-5	0.4285	2.1111E-4
4th	0.4304	2.5555E-6	0.4307	1.5097E-5	0.4309	2.1308E-4
5th	0.4313	4.1290E-6	0.4314	1.5224E-5	0.4314	2.1320E-4
6th	0.4331	4.4049E-6	0.4332	1.6088E-5	0.4334	2.8269E-4
7th	0.4336	5.2026E-6	0.4337	6.3210E-5	0.4338	7.3188E-4
8th	0.4338	8.5265E-6	0.4343	6.3592E-5	0.4351	7.3657E-4

Table 7   The value of the first several frequencies of the defect modes for the system with the PML. Total length L is 60a.

And, Table 8 tabulates the defect mode frequencies in the system with the total length equal to 40a.

For the different total length with different width of the PML, real and imaginary parts of the defect frequency both change. Generally, the longer and the thicker both make the value become higher. The increasing rate is lager for the imaginary part, which means the decay time of the field in the medium. The higher order modes, the difference between the two systems increases.

L=40	Wpml=3		Wpml=5		Wpml=8	
	Real	Imaginary	Real	Imaginary	Real	Imaginary
1st	0.4234	1.0159E-6	0.4234	5.1405E-6	0.4234	2.1440E-6
2nd	0.4258	1.6518E-6	0.4258	5.0679E-6	0.4258	7.3557E-6
3rd	0.4282	1.6635E-6	0.4283	6.5128E-6	0.4283	1.8646E-5
4th	0.4304	2.6129E-6	0.4305	8.4093E-6	0.4309	7.3024E-5
5th	0.4312	8.8797E-6	0.4314	1.0792E-5	0.4316	1.1605E-4
6th	0.4330	2.5984E-5	0.4331	6.4327E-5	0.4335	1.8544E-4
7th	0.4335	8.8272E-5	0.4337	2.0982E-4	0.4342	2.1307E-4
8th	0.4349	1.6446E-4	0.4352	8.3667E-4	0.4371	3.2649E-4

Table 8   The value of the first several frequencies of the defect modes for the system with the PML. Total

length L is 40a.

Finally, an illustration of putting the fundamental defect mode into the

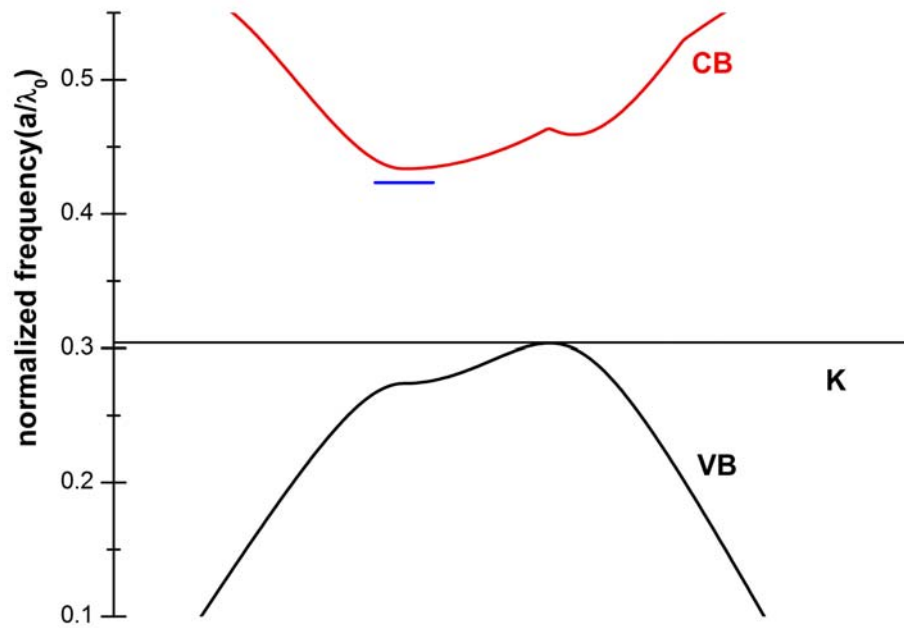photonic band structure is shown in Fig. 20.

FIG 20　The blue line specifies the fundamental defect state (ω_d =0.4234) in the photonic band structure.

5. Conclusion

This thesis proposed a novel formulation, in a form with the concept from the perfectly matched layer, to treat the envelope functions of resonant modes of localized perturbations within periodic dielectric structures. Some simulation results of the envelope of the donor type defect modes are demonstrated to discuss and optimize the performance of the parameters for the PML.

The structure of the system in this thesis consists of a 2D photonic crystal slab waveguide with a triangular array of air holes. By using the effective index method for vertical guiding, whole system is viewed as quasi-2D. Only the TE-like modes are here under discussion. And putting emphasis around the conduction band edge, several donor-type defect modes are found.

Following the work of the O. Painter's group, a decoupled and simplified Wannier envelope function is adopted. The perturbed potential is approximately designed as a parabolic potential well.

Introducing the stretched parameters in the PML into the Wannier envelope functions makes investigating the unbounded leaky modes become practical.

The simulation results with 12 sets of different settings are presented for comparison and optimization. From the results for calculating the envelope of guided modes and leaky modes, it firstly shows that the PML is suitably used to be coupled with the Wannier envelope function, not only the Maxwell' s equation. The envelope function for the leaky modes and their eigenvalue are obtained easily and efficiently. By comparing the results, it's found that the desire envelope functions and precise eigenvalues are obtained with appropriate total length of the system and thickness of the PML. Finally, some donor type defect modes are calculated and shown.

6.   Bibliography

1   Painter O. J., Husain A., Scherer A., and et al., J. Lightwave Technology, Vol.17, 1999, p.2082.

2   J. O'Brien, O. Painter, C. C. Cheng, R. Lee, A. Scherer, and A. Yariv, Electron. Lett., Vol.32, 1996, p.2243.

3   Chew W. C., and W. H. Weedon, Microwave and Optical Technology Letters, Vol.7, 1994, p.599.

4   E. M. Purcell, Phys. Rev. Vol.69, 1946, p.681.

5   D. Kleppner, Phys. Rev. Lett., Vol.47, 1981, p.233.

6   E. Yablonovitch, Phys. Rev. Lett., Vol.58, 1987, p.2059.

7   J. D. Joannopoulos, R. D. Meade, and J. N. Winn, Photonic Crystals, Princeton U. Press, Princeton, N. J., 1995.

8   S.L. McCall, P. M. Platzman, R. Dalichaouch, D. Smith, and S. Schultz, Phys. Rev. Lett., Vol.67, 1991, p.2017.

9   B. P. V. der Gaag and A. Scherer, Appl. Phys. Let., Vol.56, 1989, p.481.

10 G. Feiertag, W. Ehrfeld, H. Freimuth, H. Kolle, H. Lehr, and et. al., Appl. Phys. Lett., Vol.71, 1997, p.1443.

11 J. P. Berenger, J. Computational Phys., Vol. 114, 1994, p.185

12 C. M. Rappaport, IEEE Microwave and Guided Wave Letters, Vol.5, 1995, p.90.

13 U. Pekel, R Mittra, Microwave and optical technology letters, Vol.9, 1995, p. 117.

14 O. Painter, K. Srinviasan, P. E. Barclay, P. R. B, Vol. 68, 2003 (035214).

15 G. H. Wannier, Phys. Rev., Vol.52, 1937, p.191.

16 W. Streifer, R. D. Burnham and D. R. Scifres, Appl. Phys. Lett., Vol. 37, 1985, p.121.

17 A. Taflove, Advances in Computational Electrodynamics, Artech House Publishers, 1995.

18 M. Plihal, A. A. Maradudin, Phys. Rev. B, Vol.44, 1991, p.8565.

19 K. Ghatak, Opt. And Quan. Electrn., Vol.17, 1985, p.311.